Journal of Power Sources 196 (2011) 1399–1408

Contents lists available at ScienceDirect

Journal of Power Sources

journal homepage: www.elsevier.com/locate/jpowsour

Cathode performance of $LiMnPO_4$/C nanocomposites prepared by a combination of spray pyrolysis and wet ball-milling followed by heat treatment

The Nam Long Doan, Izumi Taniguchi*

Department of Chemical Engineering, Graduate School of Science and Engineering, Tokyo Institute of Technology, 12-1, Ookayama-2, Meguro-ku, Tokyo 152-8552, Japan

ARTICLE INFO

Article history:
Received 11 June 2010
Received in revised form 19 August 2010
Accepted 25 August 2010
Available online 28 September 2010

Keywords:
$LiMnPO_4$
Nanocomposites
Spray pyrolysis
Lithium-ion batteries
Cathode

ABSTRACT

$LiMnPO_4$/C nanocomposites could be prepared by a combination of spray pyrolysis and wet ball-milling followed by heat treatment in the range of spray pyrolysis temperature from 200 to 500 °C. The ordered $LiMnPO_4$ olivine structure without any impurity phase could be identified by X-ray diffraction analysis for all samples. It could be also confirmed from scanning electron microscopy and transmission electron microscopy observations that the final samples were the $LiMnPO_4$/C nanocomposites with approximately 100 nm in primary particles size. The $LiMnPO_4$/C nanocomposite samples were used as cathode active materials for lithium batteries, and the electrochemical tests were carried out for the cell Li|1 M $LiPF_6$ in EC:DMC = 1:1|$LiMnPO_4$/C at various charge/discharge rates in three charge modes. As a result, the final sample which was synthesized at 300 °C by spray pyrolysis showed the best electrochemical performance due to the largest specific surface area, the smallest primary particle size and a well distribution of carbon. At galvanostatic charge/discharge rates of 0.05 C, the cell delivered first discharge capacities of 123 and 165 mAh g^{-1} in correspondence to charge cutoff voltages of 4.4 and 5.0 V, respectively. Furthermore, in a constant current–constant voltage charge mode at 4.4 V, the cells also exhibited initial discharge capacities of 147 mAh g^{-1} at 0.05 C, 145 mAh g^{-1} at 0.1 C, 123 mAh g^{-1} at 1 C and 65 mAh g^{-1} at 10 C. Moreover, the cells showed fair good cycleability over 100 cycles.

1. Introduction

Since the pioneer work of Goodenough's group [1], olivine structure lithium transition-metal phosphates $LiMPO_4$ (M = Fe, Mn, Co, Ni) have been received much attention as promising cathode materials for next generation of lithium-ion batteries due to their large theoretical capacities as well as chemical and thermal stability [2–17]. In fact, $LiFePO_4$ is now considered as practical cathode material due to its excellent rate capability, which has been achieved through particle size reducing and the conductive surface coating of particles [8,10]. Recently, a numbers of studies on $LiMnPO_4$ have been reported due to the interest on its higher intercalation potential at 4.1 V versus Li^+/Li, which makes the theoretical energy density is about 1.2 times larger than that of $LiFePO_4$, and is compatible with most liquid electrolytes presently used in lithium-ion batteries. However, a poor electrochemical performance was mostly observed because of the slow lithium diffusion kinetics within the crystals and the very low intrinsic electronic conductivity which is about five orders of magnitude lower compared with that of $LiFePO_4$ [6,7]. Thus far, much effort has paid to enhance its electrochemical properties by the particle size reduction [14,18,19], the cation doping [13,20–22], the carbon coated $LiMnPO_4$ [4,11,14,23,24] or the $LiMnPO_4$/C composites [7,12,13,19–22,25–29]. On the other hand, several synthesis routes have been utilized and developed in order to overcome the weakness of $LiMnPO_4$ such as the solid-state reaction [1,5,7,22,26,27,30,31], the sol–gel method [4,19,20,32,33], the polyol process [11,12,34], the hydrothermal synthesis [21,24,35–38], microwave assisted hydrothermal method [23], solvothermal method [28,29], precipitation [6,18,25,39,40], floating-zone method [41], freeze-drying method [42] and the electrostatic spray deposition [43]. Despite of those tremendous efforts, the electrochemical performance of the $LiMnPO_4$ prepared is not sufficient for the application to commercial cells.

In our previous work [14], the carbon coated $LiMnPO_4$ could be successfully prepared by a combination of spray pyrolysis (SP) with dry ball-milling followed by heat treatment. The resulting particles have the particle size in the range from 200 to 400 nm, and a carbon layer was formed with a thickness of several tens nanometer on the surface of $LiMnPO_4$ particles. We also reported that the carbon coated $LiFePO_4$ nanoparticles [10] could be successfully synthesized by a combination of SP and wet ball-milling (WBM) with heat

* Corresponding author. Tel.: +81 3 5734 2155; fax: +81 3 5734 2155.
E-mail addresses: taniguchi.i.aa@m.titech.ac.jp, itaniguc@chemeng.titech.ac.jp (I. Taniguchi).

0378-7753/$ – see front matter © 2010 Elsevier B.V. All rights reserved.
doi:10.1016/j.jpowsour.2010.08.067

treatment. It is obvious that the WBM [10] is more effective than the dry one [9] in reducing the particle size and thus significantly improve the electrochemical performance. In the present study, the preparation of $LiMnPO_4$/C nanocomposites was conducted using a combination of SP and WBM followed by heat treatment in the range of SP temperature from 200 to 500 °C. The effect of SP temperature on physical and electrochemical properties of those materials was investigated.

2. Experimental

2.1. Precursor solution

The precursor solution was prepared by dissolving the required amounts of $LiNO_3$ (98% purity), H_3PO_4 (85% purity) and $Mn(NO_3)_2{\cdot}6H_2O$ (98% purity) in distilled water in a stoichiometric ratio. The concentrations of Li^+, Mn^{2+} and PO_4^{3-} were all 0.2 mol dm^{-3}. All chemicals were purchased from Wako Pure Chemical Industries Ltd., Japan.

2.2. Experimental setup and procedure

A schematic diagram of the SP setup was provided in our previous paper [44]. The precursor solution was atomized at a frequency of 1.7 MHz by an ultrasonic nebulizer. The sprayed droplets were transported to the reactor by a N_2 + 3% H_2 mixture gas with a gas flow rate of 2 dm^3 min^{-1}. SP temperatures were varied from 200 to 500 °C. The droplets were converted to the solid particles through a series of processes such as evaporation of solvent, precipitation of solute, drying, pyrolysis and then sintering within the laminar flow aerosol reactor. If the plug flow in the reactor is assumed, the corresponding residence time of particles inside the reactor is approximately 4.8 min. The resulting particles were collected at the reactor exit by an electrostatic precipitator operated at 170 °C.

The as-prepared $LiMnPO_4$ powders were then milled with 10 wt.% of acetylene black (electrical conductivity of 500 S m^{-1}) in ethanol by a planetary high-energy ball-milling (Fritsch, pulverisette 7). Zirconia balls and a zirconia vial were used in the WBM process. The rotating speed and ball-milling time were fixed at 800 rpm and 6 h, respectively. After the ball-milling procedure, the samples were annealed at 500 °C for 4 h in a N_2 + 3% H_2 atmosphere. Fig. 1 shows the flow chart of the preparation of $LiMnPO_4$/C nanocomposites.

2.3. Sample characterization

The crystalline phases of the samples were studied by X-ray Diffraction (XRD, Rigaku, Ultima IV with D/teX Ultra) analysis equipped with Cu Kα radiation. The lattice parameters of the material were refined by Rietveld analysis using an integrated X-ray Powder Diffraction Software Package PDXL (Rigaku, Version 1.3.0.0). The particle surface morphology was examined by field emission scanning electron microscopy (FE-SEM, Hitachi, S4500) operated at 8 kV. The interior structure of the $LiMnPO_4$/C nanocomposite particles was observed by using transmission electron microscopy (TEM, JEOL Ltd., JEM-2010F) equipped with Energy Dispersive Spectroscopy (EDS). The chemical composition of the as-prepared $LiMnPO_4$ was analyzed by Inductively Coupled Plasma Spectrometer (ICP, Shimadzu, ICPS-7510) and the specific surface area was determined by the Brunauer–Emmet–Teller method (BET, Shimadzu, Flow Sorb II 2300). The carbon content of $LiMnPO_4$/C nanocomposites was confirmed using an element analyzer (Yanaco, CHN corder MT-6). The element mapping analysis of sample was performed by Auger Electron Spectroscopy combined SEM (ULVAC-PHI Inc., PHI 680).

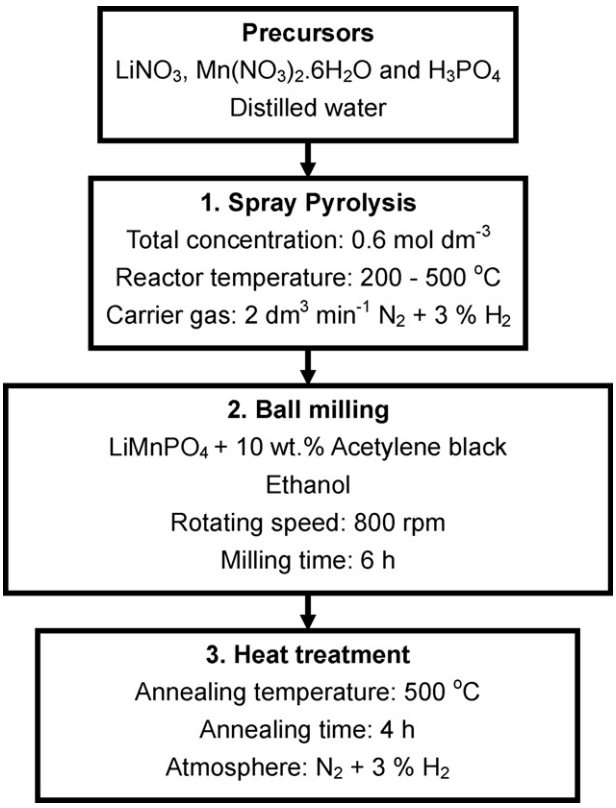

Fig. 1. Flow chart of the preparation of $LiMnPO_4$/C nanocomposites.

2.4. Electrochemical measurements

The electrochemical performance of $LiMnPO_4$/C nanocomposites was investigated using coin-type cells (CR2032). The cell is composed of a lithium metal negative electrode and a $LiMnPO_4$/C nanocomposite positive electrode that were separated by a microporous polypropylene film. 1 mol dm^{-3} solution of $LiPF_6$ in a mixed solvent of ethylene carbonate (EC) and dimethyl carbonate (DMC) with 1:1 in volume ratio (Tomiyama Pure Chemical Co., Ltd.) was used as the electrolyte. The cathode is comprised 70 wt.% $LiMnPO_4$, 10 wt.% polyvinylidene fluoride (PVdF) as a binder and 20 wt.% acetylene black, which includes the acetylene black in the $LiMnPO_4$/C nanocomposites. These materials were dispersed in 1-methyl-2-pyrrolidinone (NMP). The resultant slurry was spread uniformly onto an aluminum foil using the doctor blade technique and then dried in vacuum for 4 h at 110 °C. The cathode was punched into circular discs and then scraped in order to standardize the area of cathode (1 cm^2). The cell was assembled inside a glove box filled with high-purity argon gas (99.9995% purity). Then the cells were tested galvanostatically between 2.5 V and various charge cutoff voltages from 4.4 to 5.0 V versus Li^+/Li on multi-channel battery testers (Hokuto Denko, HJ1010mSM8A) at different charge/discharge rates from 0.05 to 10 C (1 C = 171 mAh g^{-1}). On the other hand, in the constant current–constant voltage (CC–CV) mode, the cells were charged at 0.1 C rate to 4.4 V, kept at 4.4 V until reaching theoretical capacity, and then galvanostatically discharged at different specific rates from 0.05 to 10 C. Current densities and specific capacities were calculated on the basis of the weight of $LiMnPO_4$ in the cathode.

Measurements of ac impedance spectroscopy and cyclic voltammetry were carried out using a Solartron 1255B frequency response analyzer connected to a Solartron SI 1287 electrochemical interface. The amplitude of the ac signal was 10 mV in the frequency

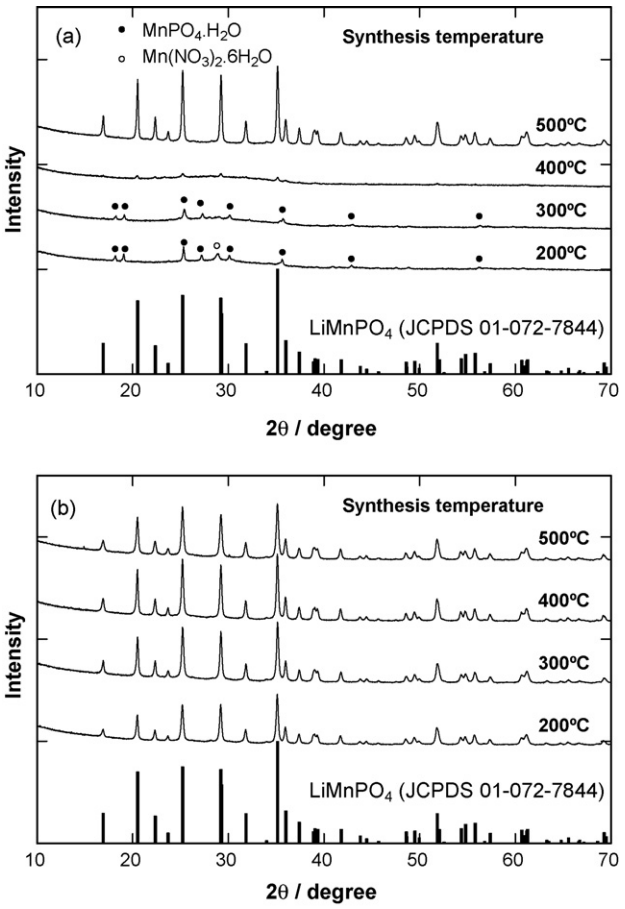

Fig. 2. XRD patterns of (a) the as-prepared $LiMnPO_4$ and (b) the $LiMnPO_4$/C nanocomposites samples synthesized by the combination of SP and WBM followed by heat treatment at different SP temperatures.

range from 100 kHz to 0.1 Hz. Cyclic voltammetry was performed between 2.5 and 4.4 V at a scanning rate of 0.05 mV s^{-1}. All electrochemical measurements were performed at room temperature.

3. Results and discussion

3.1. Effect of SP temperature on the physical properties of $LiMnPO_4$/C nanocomposites

Fig. 2a shows the XRD patterns of as-prepared samples synthesized by SP at various SP temperatures. The JCPDS card data of $LiMnPO_4$ (PDF reference number 01-072-7844) is also shown in the figure as the standard. The sample obtained at 500 °C by SP is a pure phase $LiMnPO_4$ with ordered olivine structure indexed by orthorhombic *Pmna*. Some very low intensity olivine peaks could be found on the pattern of the sample obtained at 400 °C by SP. It suggests that the crystallization may partly occur in this temperature. On the other hand, at SP temperatures of 200 and 300 °C, some impurity peaks of $MnPO_4{\cdot}H_2O$ and $Mn(NO_3)_2{\cdot}6H_2O$ could be identified. The XRD patterns of the samples synthesized by the combination of SP and WBM followed by heat treatment are presented in Fig. 2b. The diffraction peaks of all samples can be assigned to an ordered olivine structure indexed by orthorhombic *Pnma*. There is no impurity phase such as Mn_2P (JCPDS 00-002-1027). The lattice parameters of the samples obtained from Rietveld refinement are summarized in Table 1. All of the values are in good agreement with the reported data [5,12,21–23,25,28,29,33,36].

CHN analysis showed that the carbon contents are 11.7%, 11.5%, 10.8% and 10.0% for the final $LiMnPO_4$/C samples which were synthesized at SP temperatures of 200, 300, 400 and 500 °C, respectively.

Table 1
Lattice parameters of $LiMnPO_4$/C nanocomposites synthesized at different SP temperatures.

Synthesis temperature (°C)	a (Å)	b (Å)	c (Å)	V (Å^3)	$S = R_{wp}/R_p$
200	10.4390	6.1018	4.7391	301.86	1.48
300	10.4320	6.0990	4.7336	301.17	1.54
400	10.440	6.1005	4.7392	301.82	1.56
500	10.447	6.1037	4.7400	302.24	1.51

The observation of particle morphology was done by FE-SEM. The SEM images and particle size distributions of the as-prepared samples synthesized by SP at various SP temperatures are given in Fig. 3a and b, respectively. The particle size distribution measurement as well as the calculations of the geometric mean diameter $d_{g,p}$ and the geometric standard deviation σ_g were described elsewhere [44]. All samples are spherical in shape and the average particle size is approximately 1 μm. The chemical compositions of the as-prepared $LiMnPO_4$ samples were confirmed by ICP. The observed chemical compositions show fair agreement with the stoichiometric one within 3% deviation (Table 2).

The particle morphology and primary particle size distributions of the $LiMnPO_4$/C samples prepared by the present method were shown in Fig. 4. It is obvious that the primary particle size is in the range from 40 to 250 nm, which emphasizes the strong milling effect of WBM compared with the dry one [14]. From the particle size distribution (Fig. 4b), it could be observed that the final $LiMnPO_4$/C sample synthesized at 300 °C on SP has the narrowest particle size distribution $\sigma_g = 1.27$ and the smallest geometric mean diameter $d_{g,p} = 72$ nm. Fig. 5 shows the TEM observation of the final $LiMnPO_4$/C sample which was synthesized at 300 °C on SP. Both phases of carbon and $LiMnPO_4$ could be seen in this image. From the above mentioned results, we could conclude that $LiMnPO_4$/C nanocomposites could be synthesized by the combination of SP with WBM followed by heat treatment in a N_2 + 3% H_2 atmosphere.

Fig. 6 presents the variation in the observed specific surface area, $S_{LiMnPO_4/C}$, the calculated specific surface area of carbon, S_c, and the geometric mean diameter of primary particle of $LiMnPO_4$/C nanocomposites with SP temperature. The S_c was calculated by the following equations:

$$S_C = S_{LiMnPO_4/C} - S_{LiMnPO_4} \quad (1)$$

$$S_{LiMnPO_4} = \frac{6}{d_{g,p} \times \rho_C} \quad (2)$$

in which ρ_C is the crystalline density of $LiMnPO_4$ and equal to 3.4 g cm^{-3} [7]. The $LiMnPO_4$/C nanocomposite sample synthesized at 300 °C on SP shows the highest specific surface area and the smallest geometric mean diameter of primary particle. Konarova and Taniguchi [10] have already reported that the electrochemical properties of carbon coated $LiFePO_4$ nanocomposites were strongly affected by the specific surface area, and the sample with larger specific surface area showed better electrochemical performance. Furthermore, some researchers [14,18,19] reported that a reducing $LiMnPO_4$ particle size leads to the enhancement of electrochemical performance. It can be predicted from these facts that the best

Table 2
Chemical composition of as-prepared $LiMnPO_4$ powders.

Synthesis temperature (°C)	Li:Mn:P
200	1.01:0.99:1.00
300	1.00:0.97:1.00
400	1.02:1.00:1.00
500	0.98:1.00:1.00

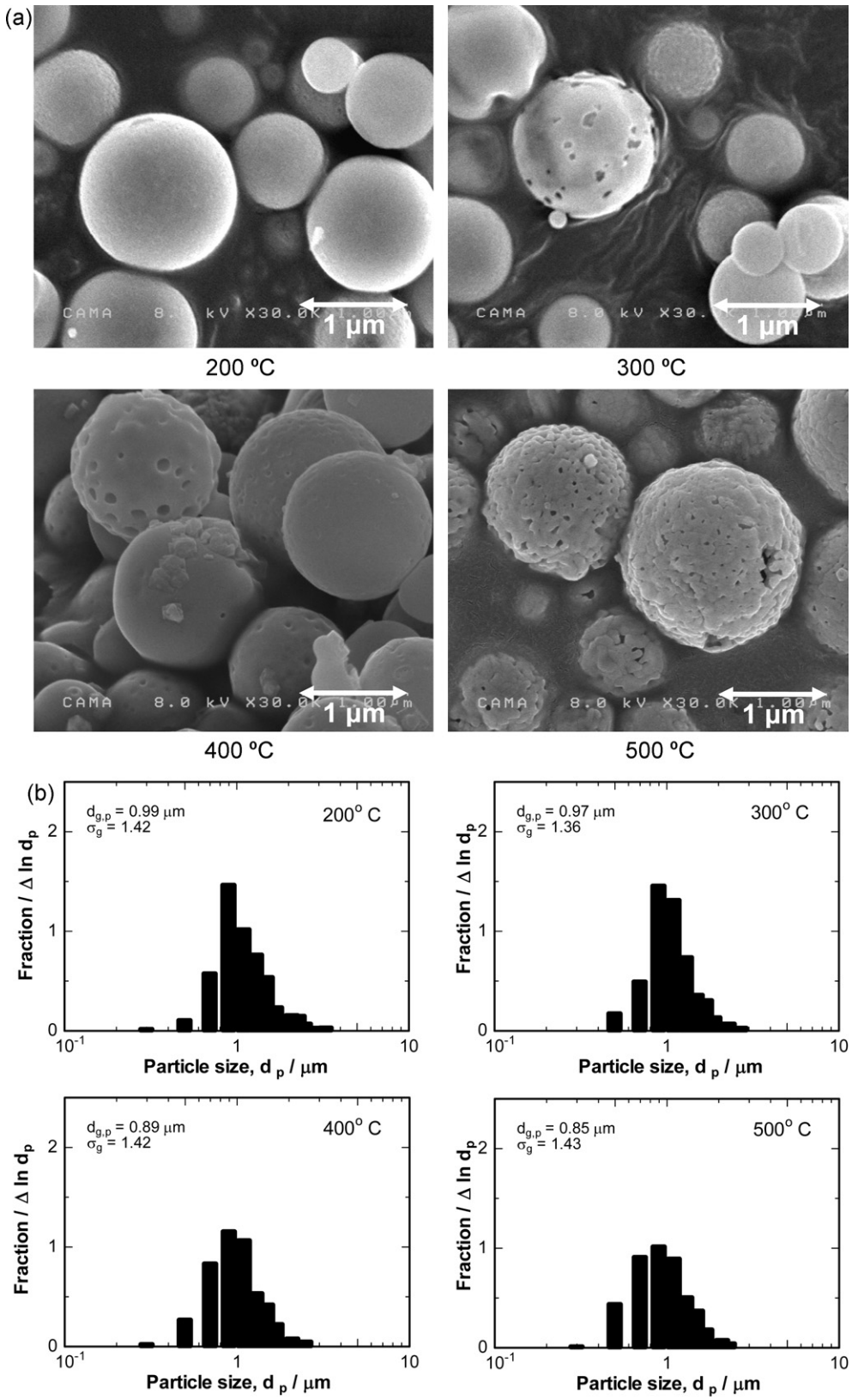

Fig. 3. (a) SEM images of the $LiMnPO_4$ synthesized by SP at different temperatures. (b) Primary particle size distributions of the $LiMnPO_4$ synthesized by SP at different SP temperatures.

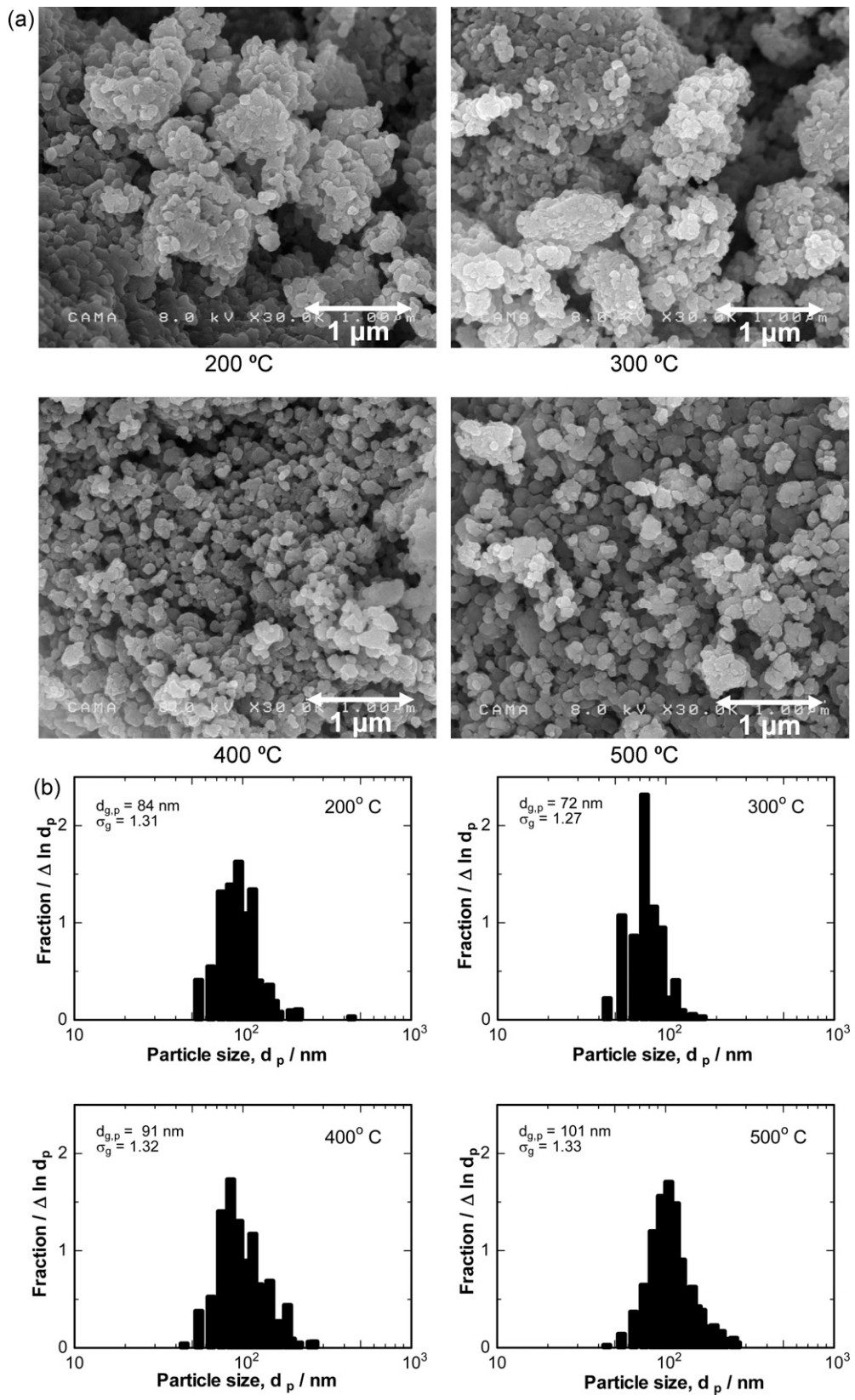

Fig. 4. (a) SEM images of the $LiMnPO_4$/C nanocomposites prepared by the combination of SP and WBM followed by heat treatment at different SP temperatures. (b) Primary particle size distributions of the $LiMnPO_4$/C nanocomposites prepared by the combination of SP and WBM followed by heat treatment at different SP temperatures.

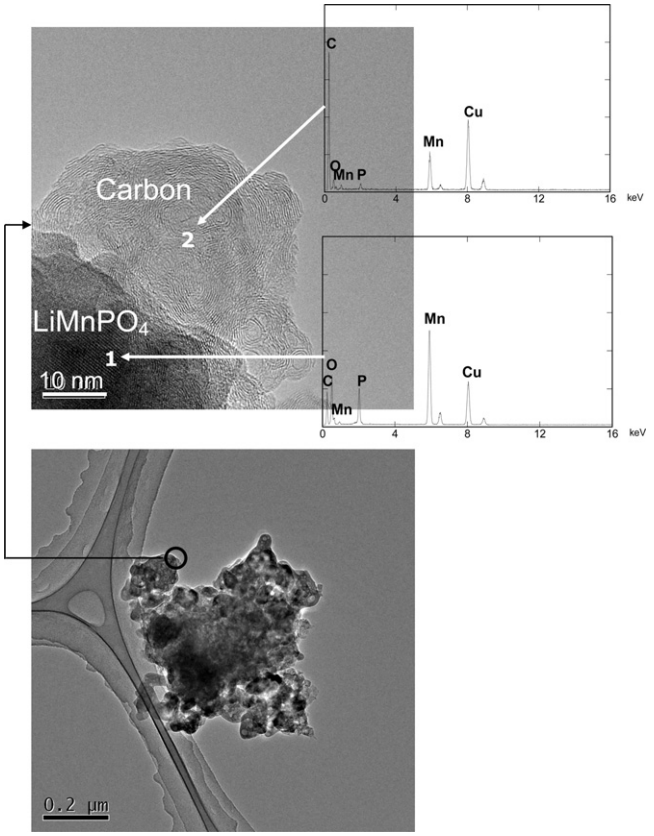

Fig. 5. TEM images of the $LiMnPO_4$/C nanocomposites prepared by the combination of SP and WBM followed by heat treatment at a SP temperature of 300 °C.

electrochemical performance could be achieved by the $LiMnPO_4$/C nanocomposites synthesized by the combination of SP and WBM with heat treatment at a SP temperature of 300 °C. In order to confirm this prediction, we investigated the electrochemical properties of the $LiMnPO_4$/C nanocomposites synthesized by the present method at different SP temperatures in the next section.

3.2. Effect of SP temperature on the electrochemical properties of $LiMnPO_4$/C nanocomposites

Fig. 7 shows the first charge/discharge profiles of the $LiMnPO_4$/C nanocomposites synthesized by the combination of SP and WBM with heat treatment at different SP temperatures. The charge/discharge rate is 0.05 C. The $LiMnPO_4$/C nanocomposite sample synthesized at 300 °C on SP delivered the largest discharge capacity (123 mAh g^{-1}). Moreover, wide flat charge/discharge plateaus could be seen at about 4.1 V region versus Li^+/Li, which extend constantly up to about 100 mAh g^{-1} with a small polarization loss. This fact may indicate that the $LiMnPO_4$/C nanocomposite is one of the best $LiMnPO_4$ cathode active materials ever reported.

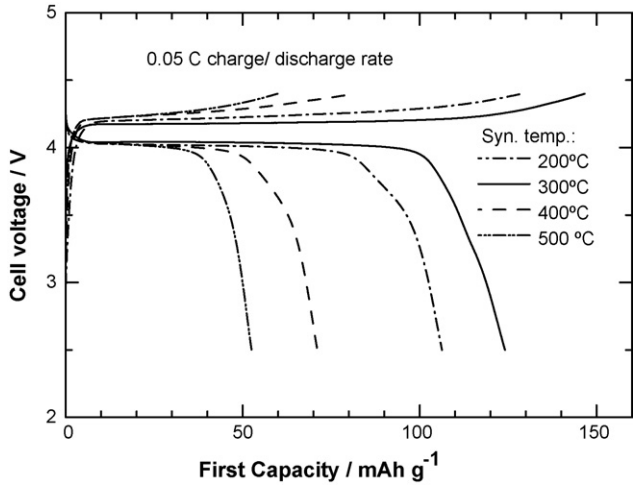

Fig. 7. First charge/discharge curves of the cells containing the $LiMnPO_4$/C nanocomposites prepared by the combination of SP and WBM followed by heat treatment at different SP temperatures.

In order to understand what make the difference in the electrochemical performance of the $LiMnPO_4$/C nanocomposites prepared by the present method at various SP temperatures, the comparison between two samples which were synthesized at 300 and 500 °C on SP was deeply investigated. Fig. 8 shows the cyclic voltammograms of the two samples. Each profile shows the oxidation and reduction peaks at about 4.3 and 3.95 V versus Li^+/Li, respectively, which correspond to the oxidation–reduction reaction of Mn^{3+}/Mn^{2+} redox couple. The pair of peaks of the $LiMnPO_4$/C nanocomposites prepared at 300 °C on SP is almost two times larger in intensity than those of the $LiMnPO_4$/C nanocomposite prepared at 500 °C on SP. Moreover, the difference in electrochemical performance becomes more obvious in ac impedance, as shown in Fig. 9.

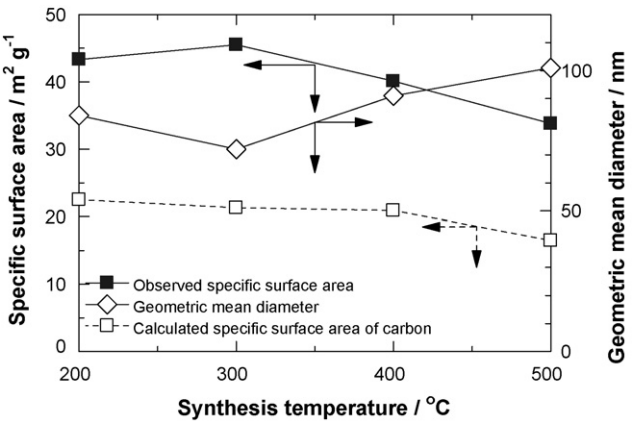

Fig. 6. Effect of SP temperature on the specific surface area and geometric mean diameter of primary particle of the $LiMnPO_4$/C nanocomposites prepared by the combination of SP and WBM followed by heat treatment at different SP temperatures.

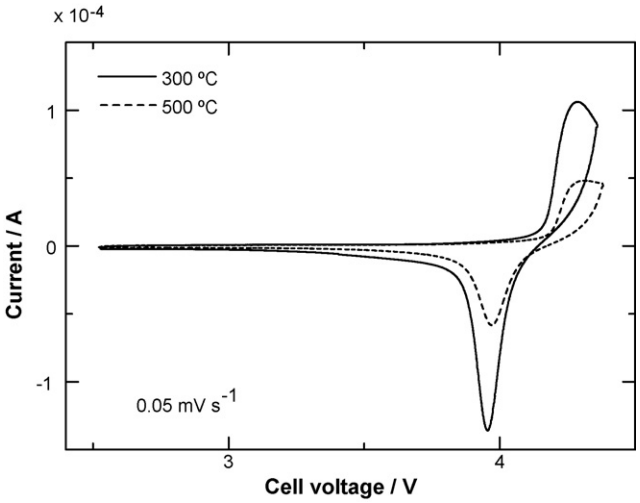

Fig. 8. Cyclic voltammograms curves of the cells containing the $LiMnPO_4$/C nanocomposites prepared by the combination of SP at 300 and 500 °C and WBM followed by heat treatment.

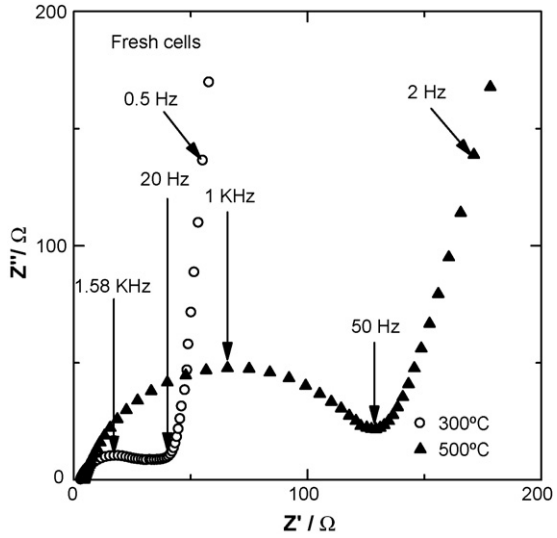

Fig. 9. Ac impedance spectra of the cells containing the $LiMnPO_4$/C nanocomposites prepared by the combination of SP at 300 and 500 °C and WBM followed by heat treatment.

Each profile is a combination of a depressed semicircle in the high to intermediate frequency region, which may represents for total charge transfer resistance in complex interfacial processes, and an inclined line in the lower frequency region represents the Warburg impedance, which related with lithium-ion diffusion in the $LiMnPO_4$ particle. The much smaller depressed semicircle could be obtained from the $LiMnPO_4$/C nanocomposites prepared at 300 °C on SP, which may indicate the smaller charge transfer resistance in the electrode–electrolyte interface of $LiMnPO_4$/C nanocomposites synthesized at 300 °C compared with the one at 500 °C.

For further explanation of the effect of SP temperatures on the electrochemical properties of $LiMnPO_4$/C nanocomposites, the element mapping analysis was conducted. Fig. 10 shows the SEM and the element (C, Mn and P) mappings of the $LiMnPO_4$/C nanocomposites synthesized at (a) 300 °C and (b) 500 °C on SP. Those of the $LiMnPO_4$ synthesized at 300 °C on SP and then annealed at 500 °C for 4 h are also shown in Fig. 10c as a reference. While the Mn and P distributions are similar among three samples, it is obvious that the carbon distribution of the $LiMnPO_4$/C nanocomposites prepared at 300 °C on SP is more uniform than the one at 500 °C on SP. From above characterizations and discussion, it can be concluded that the $LiMnPO_4$/C nanocomposites synthesized by the present method at a SP temperature of 300 °C have the best electrochemical performance, due to the highest specific surface area, the smallest primary particle size and a well distribution of carbon.

3.3. Cycleability and rate capability of the $LiMnPO_4$/C nanocomposites synthesized by the combination of SP and WBM with heat treatment at a SP temperature of 300 °C

The cycle performance of the cells containing $LiMnPO_4$/C nanocomposites was evaluated at different C rates such as 0.2, 0.5 and 1 C (Fig. 11a) using constant current (CC) charge mode up to 4.4 V (CC-4.4 V). While the cell showed almost no remarkable gain or loss of discharge capacity at 1 C, the discharge capacity retentions were 80% and 92% at 0.2 and 0.5 C rates after 100 cycles, respectively. Beside the electrolyte decomposition, capacity fading might be due to the structure volume change during charge/discharge processes, which may reduce the effective contact area between carbon and $LiMnPO_4$. At low C rates such as 0.2 C, the charge and discharge capacities are large, which lead to large structure volume change. Therefore, more serious capacity fading might occur at lower charge–discharge rate. However, in general, the cells showed fair good cycleability over 100 cycles.

The first charge–discharge profiles of the cells containing $LiMnPO_4$/C nanocomposites at different charge cutoff voltages of 4.4, 4.6, 4.8 and 5 V are shown in Fig. 12a. It could be seen here that the charge curve is extended with increasing the charge cut-

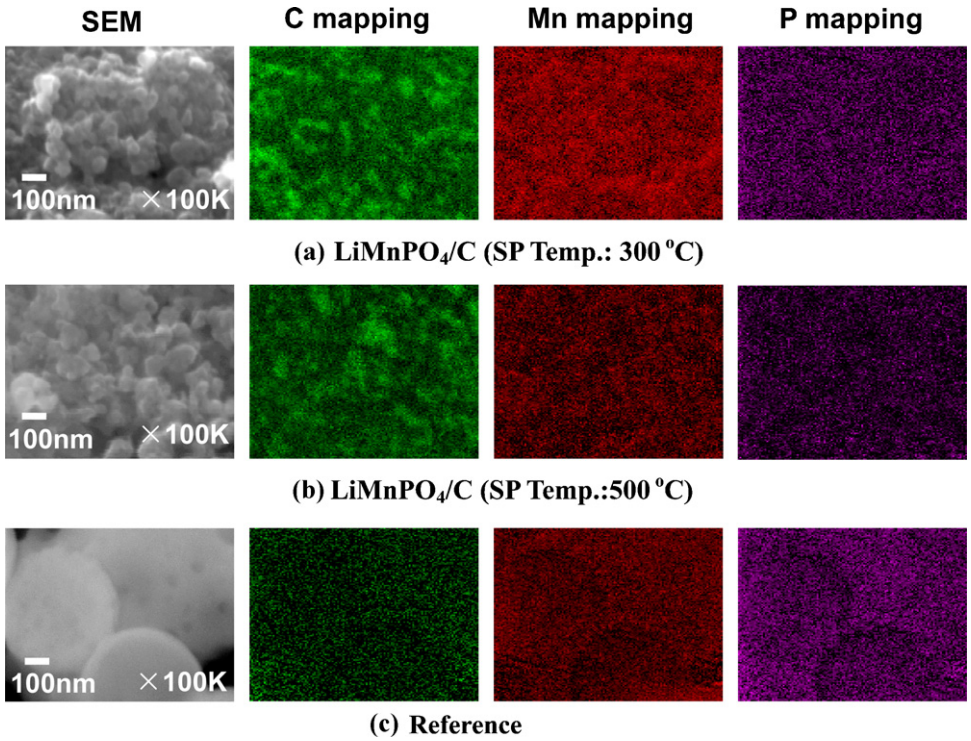

Fig. 10. Element mappings of the $LiMnPO_4$/C nanocomposites prepared by the combination of SP at (a) 300 °C and (b) 500 °C and WBM followed by heat treatment and (c) the $LiMnPO_4$ synthesized by SP at 300 °C followed by heat treatment.

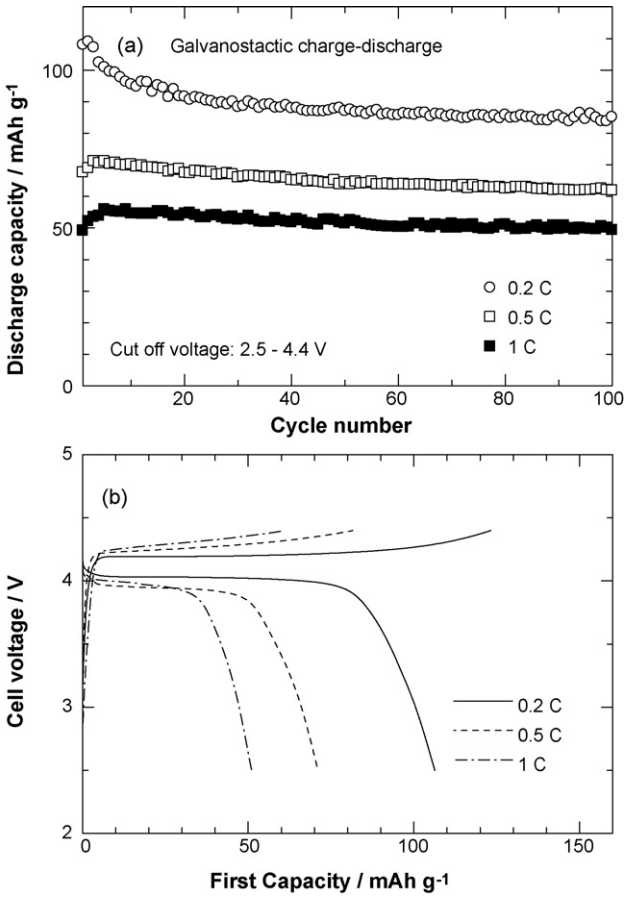

Fig. 11. (a) Cycle performance and (b) first charge/discharge curves at various C rates of the cells containing the $LiMnPO_4$/C nanocomposites prepared by the combination of SP at 300 °C and WBM followed by heat treatment.

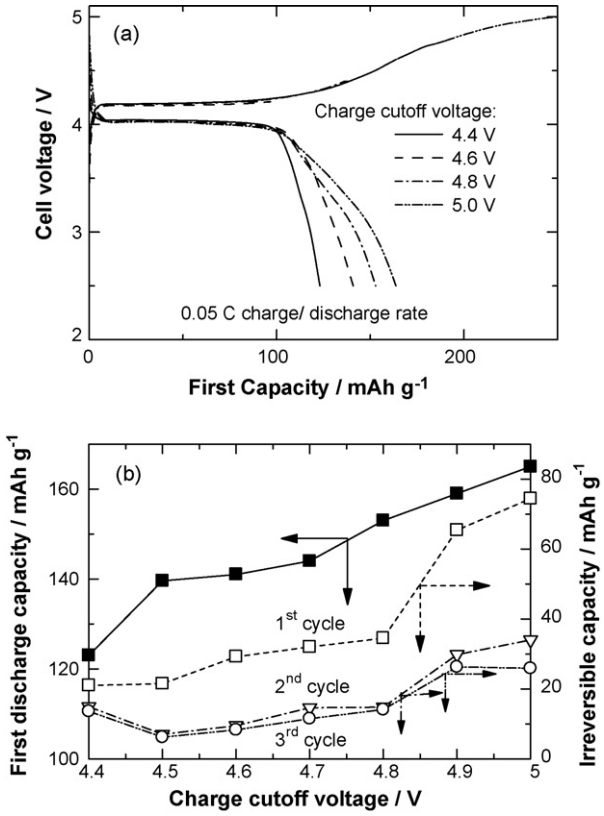

Fig. 12. (a) Effect of charge cutoff voltages on the first charge/discharge curves of the cells containing the $LiMnPO_4$/C nanocomposites prepared by the combination of SP at 300 °C and WBM followed by heat treatment. (b) Effect of charge cutoff voltage on the first discharge capacity, the first, second and third irreversible capacities of the cells containing the $LiMnPO_4$/C nanocomposites prepared by the combination of SP at 300 °C and WBM followed by heat treatment.

off voltage. Thus, the discharge capacity also increases due to the deeper level of lithium extraction and the longer charge stage. As a consequence, the cell delivered first discharge capacities of 123 and 165 mAh g^{-1} in correspondence to charge cutoff voltages of 4.4 and 5.0 V, respectively. Fig. 12b presents the effect of charge cutoff voltage on the initial discharge capacity and the first, second and third irreversible capacities. The first discharge capacity drastically increases with a charge cutoff voltage from 4.4 to 4.5 V and then gradually increases with a charge cutoff voltage from 4.5 to 5.0 V. On the other hand, the irreversible capacities also become larger with higher charge cutoff voltage. It is noted here that the first irreversible capacity is much larger than the second and the third ones, due to the side reactions of the electrolyte with carbon at operating voltage higher than 4.3 V in the initial charge state [11]. From these results, the charge cutoff voltage of 4.8 V (CC-4.8 V) could be considered as the practical choice since the sample delivered sufficient initial discharge capacity with relatively low irreversible capacity.

Fig. 13 shows the initial charge/discharge profiles of the cells evaluated at CC–CV charge mode up to the cutoff voltage of 4.4 V (CC–CV-4.4 V) and various CC discharge rates. The flat discharge plateau is still clearly recognized even at high C rate such as 2 C, due to the deep Li extraction level under very low currents in constant voltage (CV) charge stage.

Fig. 14 shows the rate capability of the cells containing $LiMnPO_4$/C nanocomposites which were performed at three charge modes: CC-4.4 V, CC-4.8 V, and CC–CV-4.4 V. At the discharge rate of 0.05 C, these cells exhibited the first discharge capacities of 123, 153 and 147 mAh g^{-1} in CC-4.4 V, CC-4.8 V and CC–CV-4.4 V charge modes, respectively. At higher C rate such as 1 C, the initial discharge capacities of 51, 107 and 123 mAh g^{-1} were observed in correspondent to CC-4.4 V, CC-4.8 V and CC–CV-4.4 V charge modes, respectively. Even at much higher C rate such as 10 C, the cell still worked and could deliver 65 mAh g^{-1} at CC–CV-4.4 V charge mode. The present cells included $LiMnPO_4$/C nanocomposites exhibited a very good rate capability despite of the intrinsic very low electronic and ionic conductivity of $LiMnPO_4$.

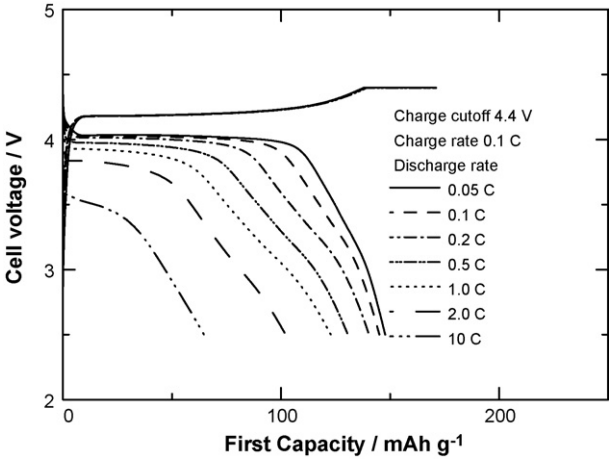

Fig. 13. First charge/discharge curves at CC–CV charge condition of the cells containing the $LiMnPO_4$/C nanocomposites prepared by the combination of SP at 300 °C and WBM followed by heat treatment.

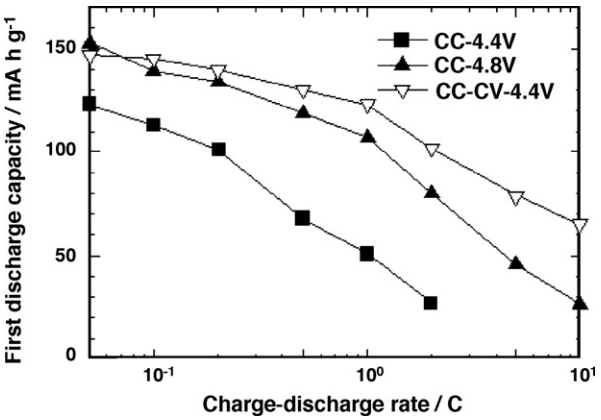

Fig. 14. Rate capability of the cells containing the $LiMnPO_4$/C nanocomposites prepared by the combination of SP at 300 °C and WBM followed by heat treatment.

Table 3
Comparison of first specific capacities of $LiMnPO_4$/C nanocomposites of this study and previous reported data at room temperature.

Samples	C rate	Cutoff voltages (V)	Charge mode	Discharge capacity ($mAh\,g^{-1}$)
This study	0.1 C	2.5–4.4	CC–CV	145
Ref. [12]	0.1 C	2.7–4.4	CC–CV	141
Ref. [22]	0.1 C	2.7–4.4	CC–CV	95
Ref. [39]	0.05 C	2.5–4.4	CC–CV	115
This study	0.05 C	2.5–4.8	CC	153
Ref. [6]	0.05 C	2.0–4.9	CC	96
Ref. [28]	0.01 C	2.4–4.8	CC	127
Ref. [45]	0.05 C	3.0–4.8	CC	145

Table 3 shows the comparison of $LiMnPO_4$/C nanocomposites prepared in this study with previous works, which clearly indicates that the $LiMnPO_4$/C nanocomposite is one of the best $LiMnPO_4$ cathode active materials ever reported. This good performance could be clearly explained by the large specific surface area, the small primary particle size and a well distribution of carbon.

The cycle performance comparison between three charge modes also was shown in Fig. 15. The cells containing $LiMnPO_4$/C nanocomposites showed good cycle performance despite the use of different charge modes.

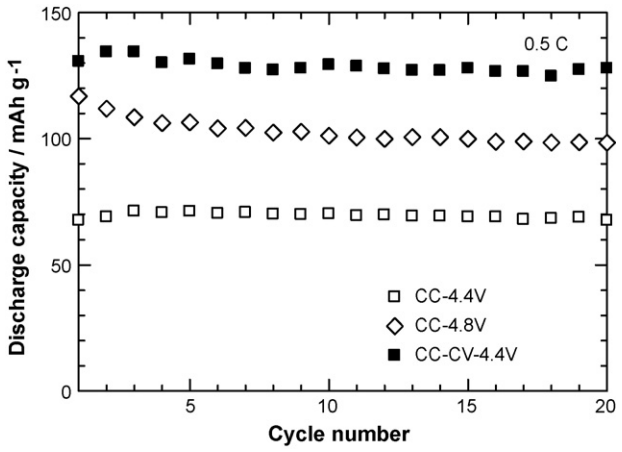

Fig. 15. Cycle performance at different charge modes of the cells containing the $LiMnPO_4$/C nanocomposites prepared by the combination of SP at 300 °C and WBM followed by heat treatment.

4. Conclusions

$LiMnPO_4$/C nanocomposites could be successfully prepared by the combination of SP with WBM followed by heat treatment in a N_2 + 3% H_2 atmosphere. XRD patterns of all samples could be identified as single phase ordered $LiMnPO_4$ olivine structure indexed by orthorhombic *Pmna*. It could be also confirmed from SEM and TEM observations that the final samples were the $LiMnPO_4$/C nanocomposites with approximately 100 nm in primary particles size. The $LiMnPO_4$/C nanocomposites were used as cathode active materials for lithium-ion batteries, and electrochemical performance was investigated using the Li|1 M $LiPF_6$ in EC:DMC = 1:1|$LiMnPO_4$/C cells at room temperature. The sample which was synthesized by the combination of SP and WBM with heat treatment at a SP temperature of 300 °C showed the best electrochemical performance due to the largest specific surface area, the smallest geometric mean diameter of primary particle and a well distribution of carbon. At a charge/discharge rates of 0.05 C, the cells exhibited first discharge capacities of 123 and 165 $mAh\,g^{-1}$ in correspondence to charge cutoff voltages of 4.4 and 5.0 V, respectively. On the other hand, using CC–CV-4.4 V charge mode, the cell also exhibited an initial discharge capacity of 147 $mAh\,g^{-1}$ at 0.05 C, 145 $mAh\,g^{-1}$ at 0.1 C, 123 $mAh\,g^{-1}$ at 1 C and 65 $mAh\,g^{-1}$ at 10 C. Moreover, the cell showed fair good cycleability over 100 cycles.

Acknowledgements

This work was supported by the Development of an Electric Energy Storage System for Grid-connection with New Energy Resources in New Energy and Industrial Technology Development Organization. The authors are grateful to the staff members (Mr. A. Hori and Mr. J. Koki) of the Center for Advanced Materials Analysis (Tokyo Institute of Technology, Japan) for the FE-SEM and TEM observations of samples.

References

[1] A.K. Padhi, K.S. Nanjundaswamy, J.B. Goodenough, J. Electrochem. Soc. 144 (1997) 1188.
[2] F. Zhou, M. Cococcioni, K. Kang, G. Ceder, Electrochem. Commun. 6 (2004) 1144.
[3] D. Morgan, A. Van der Ven, G. Ceder, Electrochem. Solid-State Lett. 7 (2004) A30.
[4] J. Yang, J.J. Xu, J. Electrochem. Soc. 153 (2006) A716.
[5] C.M. Julien, A.A. Salah, F. Gendron, J.F. Morhange, A. Mauger, C.V. Ramana, Scripta Mater. 55 (2006) 1179.
[6] C. Delacourt, L. Laffont, R. Bouchet, C. Wurm, J.-B. Leriche, M. Morcrette, J.-M. Tarascon, C. Masquelier, J. Electrochem. Soc. 152 (2005) A913.
[7] M. Yonemura, A. Yamada, Y. Takei, N. Sonoyama, R. Kanno, J. Electrochem. Soc. 151 (2004) A1352.
[8] B. Kang, G. Ceder, Nature 458 (2009) 190.
[9] M. Konarova, I. Taniguchi, Powder Technol. 191 (2009) 111.
[10] M. Konarova, I. Taniguchi, J. Power Sources 195 (2010) 3661.
[11] S.K. Martha, B. Markovsky, J. Grinblat, Y. Gofer, O. Haik, E. Zinigrad, D. Aurbach, T. Drezen, D. Wang, G. Deghenghi, I. Exnar, J. Electrochem. Soc. 156 (2009) A541.
[12] D. Wang, H. Buqa, M. Crouzet, G. Deghenghi, T. Drezen, I. Exnar, N.-H. Kwon, J.H. Miners, L. Poletto, M. Grätzel, J. Power Sources 189 (2009) 624.
[13] T. Shiratsuchi, S. Okada, T. Doi, J. Jamaki, Electrochim. Acta 54 (2009) 3145.
[14] T.N.L. Doan, Z. Bakenov, I. Taniguchi, Adv. Powder Technol. 21 (2010) 187.
[15] N.N. Bramnik, K.G. Bramnik, C. Baehtz, H. Ehrenberg, J. Power Sources 145 (2005) 74.
[16] N.N. Bramnik, K. Nikolowski, D.M. Trots, H. Ehrenberg, Electrochem. Solid-State Lett. 11 (2008) A89.
[17] M.E. Rabanal, M.C. Gutierrez, F. Garcia-Alvarado, E.C. Gonzalo, M.E. Arroyo-de Dompablo, J. Power Sources 160 (2006) 523.
[18] C. Delacourt, P. Poizot, M. Morcrette, J.-M. Tarascon, C. Masquelier, Chem. Mater. 16 (2004) 93.
[19] T. Drezen, N.-H. Kwon, P. Bowen, I. Teerlinck, M. Isono, I. Exnar, J. Power Sources 174 (2007) 949.
[20] R. Dominko, M. Bele, M. Gaberscek, M. Remskar, D. Hanzel, J.M. Goupil, S. Pejovnik, J. Jamnik, J. Power Sources 153 (2006) 274.
[21] G. Chen, J.D. Wilcox, T.J. Richardson, Electrochem. Solid-State Lett. 11 (2008) A190.
[22] D. Wang, C. Ouyang, T. Drézen, I. Exnar, A. Kay, N.-H. Kwon, P. Gouerec, J.H. Miners, M. Wang, M. Grätzel, J. Electrochem. Soc. 157 (2010) A225.

[23] A.V. Murugan, T. Muraliganth, A. Manthiram, J. Electrochem. Soc. 156 (2009) A79.
[24] Y. Mizuno, M. Kotobuki, H. Munakata, K. Kanamura, J. Ceram. Soc. Jpn. 117 (2009) 1225.
[25] N.N. Bramnik, H. Ehrenberg, J. Alloys Compd. 464 (2008) 259.
[26] G. Li, H. Azuma, M. Tohda, Electrochem. Solid-State Lett. 5 (2002) A135.
[27] M. Minakshi, P. Singh, S. Thurgate, K. Prince, Electrochem. Solid-State Lett. 9 (2006) A471.
[28] Y. Wang, Y. Yang, Y. Yang, H. Shao, Solid State Commun. 150 (2010) 81.
[29] Y. Wang, Y. Yang, Y. Yang, H. Shao, Mater. Res. Bull. 44 (2009) 2139.
[30] A. Yamada, M. Hosoya, S.-C. Chung, Y. Kudo, K. Hinokuma, K.-Y. Liu, Y. Nishi, J. Power Sources 119 (2003) 232.
[31] S. Okada, S. Sawa, M. Egashira, J. Yamaki, M. Tabuchi, H. Kageyama, T. Konishi, A. Yoshino, J. Power Sources 97–98 (2001) 430.
[32] D. Arčon, A. Zorko, P. Cevc, R. Dominko, M. Bele, J. Jamnik, Z. Jagličić, I. Golosovsky, J. Phys. Chem. Solids 65 (2004) 1773.
[33] M. Piana, B.L. Cushing, J.B. Goodenough, N. Penazzi, Solid State Ionics 175 (2004) 233.
[34] T.R. Kim, D.H. Kim, H.W. Ryu, J.H. Moon, J.H. Lee, S. Boo, J. Kim, J. Phys. Chem. Solids 68 (2007) 1203.
[35] J. Chen, S. Wang, M.S. Whittingham, J. Power Sources 174 (2007) 442.
[36] H. Fang, Z. Pan, L. Li, Y. Yang, G. Yan, G. Li, S. Wei, Electrochem. Commun. 10 (2008) 1071.
[37] S.-W. Kim, J. Kim, H. Gwon, K. Kang, J. Electrochem. Soc. 156 (2009) A635.
[38] G. Chen, T.J. Richardson, J. Power Sources 195 (2010) 1221.
[39] J. Xiao, W. Xu, D. Choi, J.-G. Zhang, J. Electrochem. Soc. 157 (2010) A142.
[40] C. Delacourt, C. Wurm, P. Reale, M. Morcrette, C. Masquelier, Solid State Ionics 173 (2004) 113.
[41] N. Wizent, G. Behr, F. Lipps, I. Hellmann, R. Klingeler, V. Kataev, W. Löser, N. Sato, B. Büchner, J. Cryst. Growth 311 (2009) 1273.
[42] V. Koleva, R. Stoyanova, E. Zhecheva, Mater. Chem. Phys. 121 (2010) 370.
[43] J. Ma, Q.-Z. Qin, J. Power Sources 148 (2005) 66.
[44] I. Taniguchi, Mater. Chem. Phys. 92 (2005) 172.
[45] B. Kang, G. Ceder, J. Electrochem. Soc. 157 (2010) A808.